Supplementary Information:

Morphological intelligence counters foot slipping in the desert locust and dynamic robots

Matthew A. Woodward[1] and Metin Sitti[1]

[1] *Physical Intelligence Department, Max Planck Institute for Intelligent Systems, Stuttgart, Germany*
woodward@is.mpg.de, sitti@is.mpg.de

This PDF file includes:

Sections S1 to S3
Figs. S1 to S5
Movies 1 to 4

www.pnas.org/cgi/doi/10.1073/pnas.1804239115

Supplementary Information

S1 Jumping Adaptation

The morphology of the locust's hind legs used for jumping, exhibit striking similarity to that of the 4 forelegs (Fig. S1c). The forelegs also have 4 jointed tibia spines and 3 segment feet with 3 adhesive pads on the first segment, $S1$; however, their configurations are better configured to enhance foot holds during rapid running over challenging surfaces. The spines are smaller, conical shaped, and pointed more distally than in the hind legs, and the adhesive pad have no separation between pads $P1$ and $P2$. These morphological similarities add additional evidence to the hypothesis of the locust's continued adaptation towards enhanced jumping performance.

S2 Foot Bouncing

A two-body jumping simulation was developed (Fig. S5c and MM: Dynamics). The leg compliance caused by the driving spring, similar to series elastic actuation,[78] provides significant energy absorption from impacts. However, in addition, integrated into the kinematic chain of the leg and foot are several 3D-printed ABS (Stratasys uPrintSE Plus, ABSplus) components, which have a relatively low coefficient of restitution, $COR = 0.8929$; experimentally determined in Appendix: Material Properties. This acts as the buckling region in the locust's leg, dissipating some of the impact energy of the foot, c_2, which reduces bouncing, facilitating surface interaction, Fig. S5d; other effects such as adhesion, interlocking, and the elastomer foot pads will add additional damping, whereas the foot mass, m_F, is directly related to the bouncing amplitude and should be minimized.

It is difficult to observe bouncing in the robotic experiments with the SLIP foot as the expected size scale is relatively small. However, during non-contact jumps, small oscillations can sometimes be observed not at the interface but in the foot itself, which may indicate the expected minor bouncing. These oscillations are damped within a few cycles due to the added damping of the entire kinematic chain with integrated low COR components and the soft elastomer foot pads. The asymmetric foot however, results in significant bouncing (Fig. S3c) due to its higher rotational and thus impact velocities; the overall behavior is also observed to be less stable than that of the symmetric foot.

S3 Material Properties

Two properties of the 3D-printed ABS material (Stratasys, ABSplus) were determined experimentally including: coefficient of restitution and Young's modulus.

The coefficient of restitution (COR) was experimentally calculated by colliding two equal spheres together and comparing the energy before and after the collision. Figure S5e shows the testing setup for determining the COR of the material; where the two spheres are identical and the height potential energy before and after the collision is used to calculate the COR, $COR = 0.8929$.

The Young's modulus of the material was experimentally tested to obtain the modulus for thin small sections. The manufacturing process of the uPrintSE (Stratasys) results in significant differences between bulk and small sections. The test consisted of two printed cantilever beams with dimensions (LxWxH): 40x1x3 mm and 40x3x1 mm. Each was loaded and the deformation measured. Using the Euler-Bernoulli beam theory, the Young's moduli for each configuration was calculated as, 173.25 MPa and 164.77 MPa, respectively.

References

[78] Pratt GA, Williamson MM (1995) Series elastic actuators. *IEEE/RSJ International Conference on Intelligent Robots and Systems* pp 399–406.

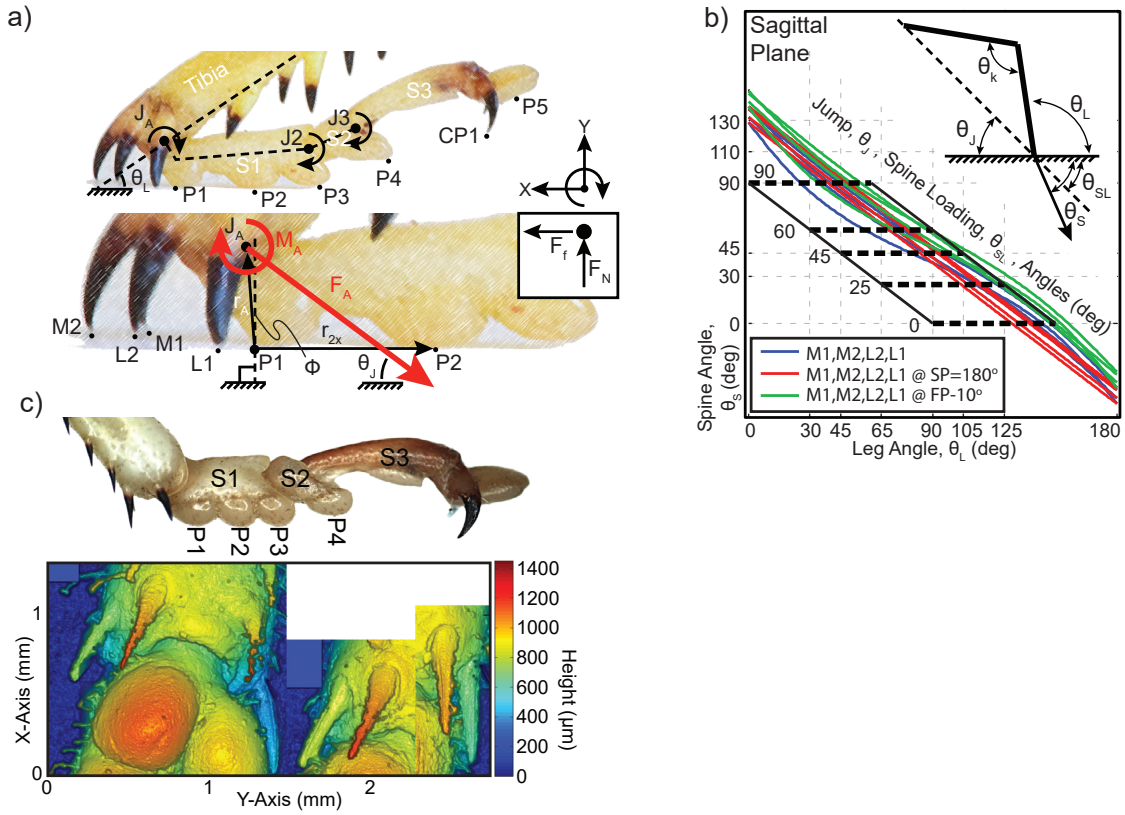

Figure S1: Locust's feet. **a)** Locust foot diagram. **b)** Spine orientation plot which shows the relationship between leg, θ_L, spine, θ_S, jumping, θ_J, and spine loading, $\theta_{SL} = \theta_J$, angles; where $\theta_S \leq 0$ indicates the spine tip is not longer able to interact with the surface (MM: Spine Orientation). **c)** The forefeet of the locust, morphologically similar to the hind feet, albeit with underdeveloped spines and passive joints at the base (photo and 3D surface profilometer micrographs).

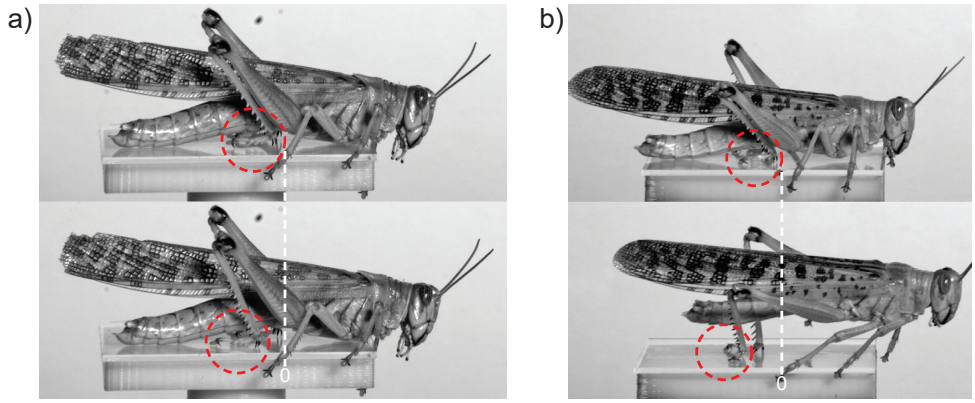

Figure S2: Locust's specific jump behaviors. **a)** Non-contact jump, where the foot dynamically engages the surface (high-speed video snapshots). Note the reflection of the adhesive pad in the glass highlighting the existence of a gap. **b)** Type-3 slip in the locust; rarely observed (high-speed video snapshots). **Note:** Motion of the red circle represents the approximate motion of the feature in the two images.

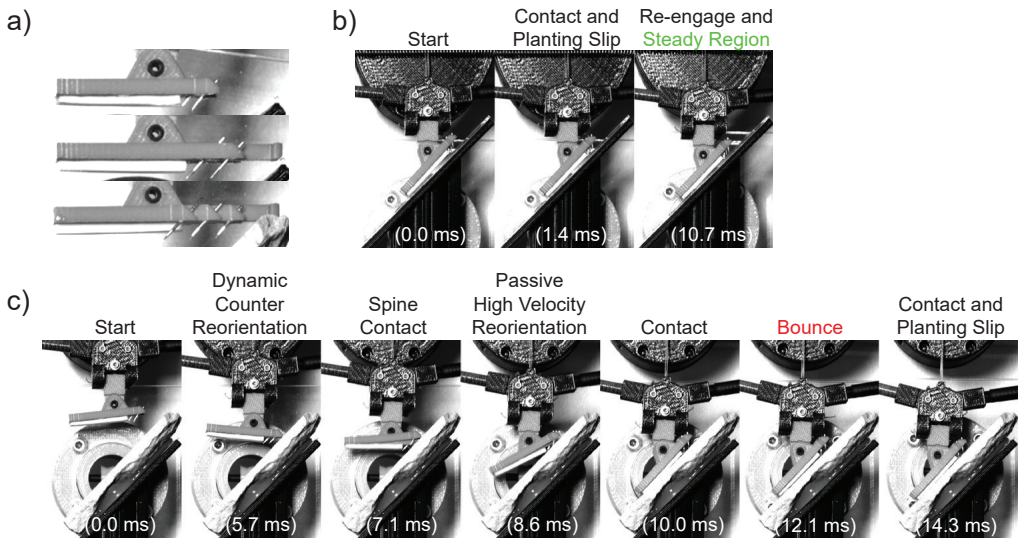

Figure S3: Robot experimental trials for asymmetric feet (similar to locust morphology) with coupled spine and adhesive pad rotations on the two most difficult surfaces. **a)** Additional feet with increasing spine loading (video snapshots). **b)** Contact jump (glass). (high-speed video snapshots) **c)** Non-contact jump (sandstone). (high-speed video snapshots)

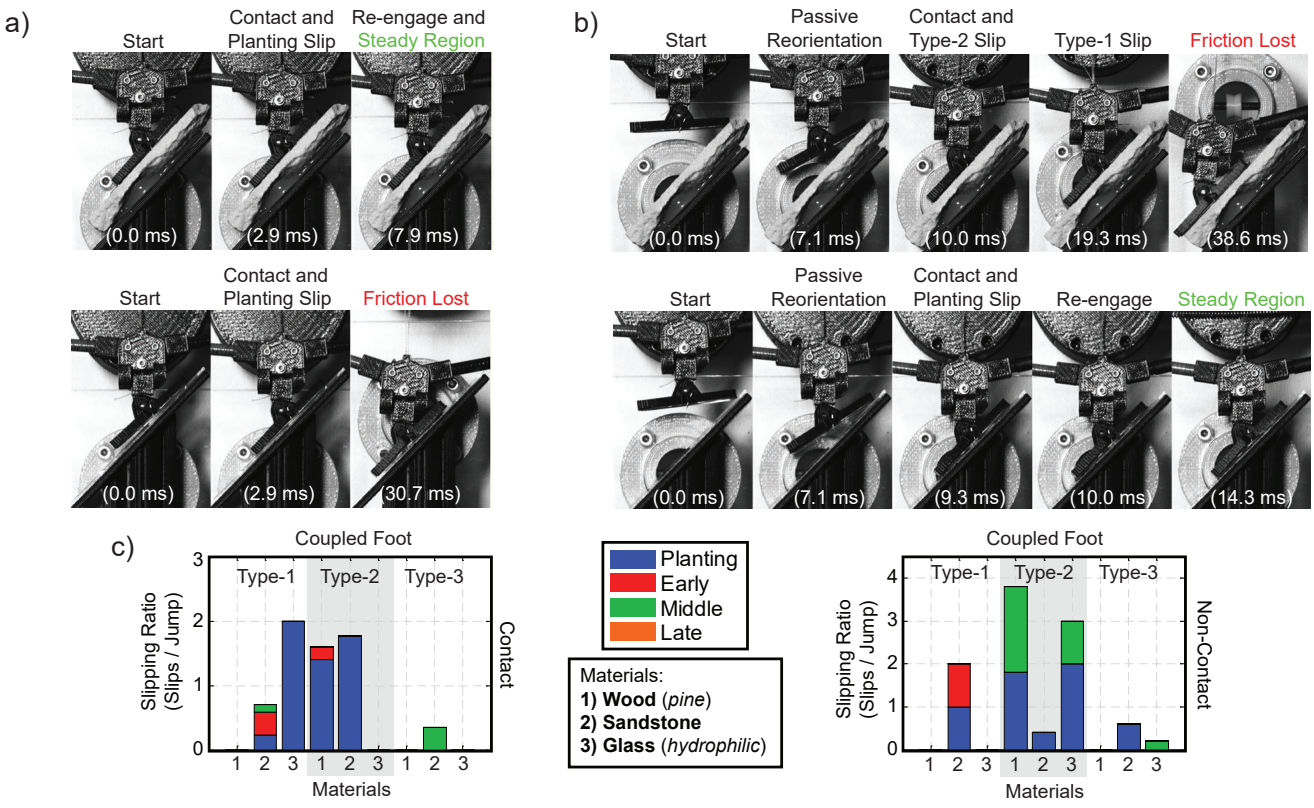

Figure S4: Robot experimental results for the symmetric foot with coupled spine and adhesive pad rotations on the two most difficult surfaces. **a)** Contact jumps (sandstone, glass). (high-speed video snapshots) **b)** Non-contact jumps (sandstone, glass). (high-speed video snapshots) **c)** Experimental results per jump (per leg rates are half), for the contact and non-contact jump trials.

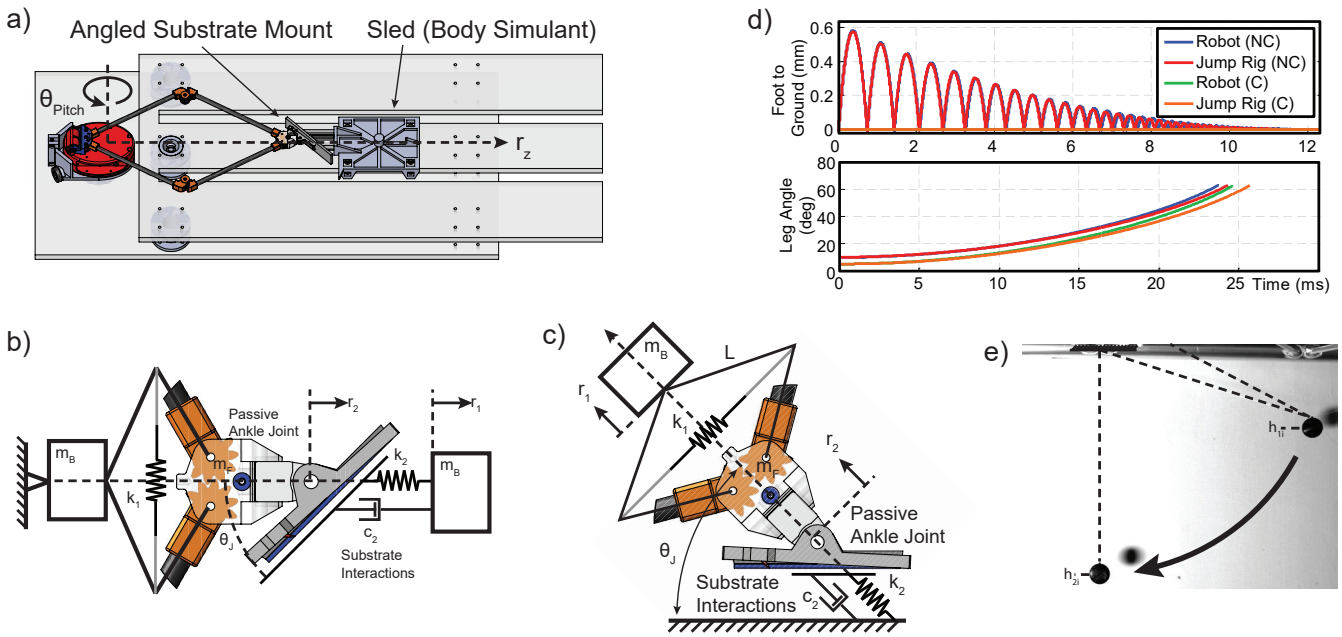

Figure S5: Robot experimental setup and material characterization. **a)** Dynamically similar jump testing rig. **b)** The free body diagram of the jumping rig. **c)** The free body diagram of the robotic platform. **d)** Dynamic comparison between the jumping rig and the robot. Both the bouncing of the foot and jumping behavior are presented to show the similarity. Note: NC=non-contact jump, C=contact jump. **e)** A pendulum setup was used to experimentally determine the coefficient of restitution of the 3D printed ABS plastic (Stratasys, ABSplus). Superimposed high-speed video snapshots.

Movie 1: Locust jumping trials (high speed videos). First is an example of three slips in a single trial; highlighting the concept of multiple slips. Second are four simultaneous trials; highlighting the variability of the surfaces, jumping, and slipping. The examples trials, however, do not represent average behaviors on the surfaces.

Movie 2: Image of the MultiMo-Bat shown alongside an animation of the SLIP foot orienting and engaging a surface. The motion of the foot is shown to highlight the decoupling of the rotational motion of the leg, adhesive pad, and spines.

Movie 3: Example of a rare type-3 slip in the locust (high speed video); it is followed by a type-1 slip.

Movie 4: Robot jumping trials (high speed videos). First are examples of the contact and non-contact jumping trials of the robot on the glass, wood, and sandstone surfaces. Second are MultiMo-Bat experiments, for 45° surface angles, showing similar performances between the surfaces; followed by experiments at twice the energy (80% increase in energy density due to an additional 13.2 g), comparing the flat performance to that of type-3 slipping on wood at a 45° surface angle.